Fabrication of $Bi_{0.5}(Na_{0.4}K_{0.1})TiO_3$ Lead-Free Ceramics Using Reactive Templated Grain Growth Method for Improving Their Preferred Degree of Orientation, Dielectric, and Ferroelectric Properties

LE DAI VUONG ⓘ,[1,5] DAO ANH QUANG,[2,6] PHAM VAN QUAN,[3] and NGUYEN TRUONG-THO[4]

1.—Faculty of Natural Sciences, Thu Dau Mot University, Binh Duong Province, Vietnam. 2.—Institute of Research and Development, Duy Tan University, Da Nang 550000, Vietnam. 3.—Hue Industrial College, Hue City, Vietnam. 4.—College of Sciences, Hue University, Hue City, Vietnam. 5.—e-mail: ledaivuong@tdmu.edu.vn. 6.—e-mail: daoanhquang@duytan.edu.vn

A $Bi_4Ti_3O_{12}$ template was added to the $(1 - x)[Bi_{0.5}(Na_{0.4}K_{0.1})TiO_3]$-$xBi_4Ti_3O_{12}$ ceramics (BNKT; where $x = 0$, 0.1, 0.15, 0.20, 0.25, and 0.30) and lead-free ceramics were produced by tape casting to improve their dielectric and ferroelectric properties. X-ray diffraction patterns and Raman scattering spectra showed a pure perovskite phase in the all-ceramic samples. In addition, the surface morphology of BNKT ceramics was identified by microstructure images. The experimental results demonstrated that the textured BNKT ceramics exhibited improved electrical properties and achieved expected values at $x = 0.15$: the highest density ρ of 6.19 g/cm^3 (relative density of 98% of the theoretical), dielectric constant ε_{max} of 6680, high remnant polarization (P_r) of 16 μC/cm^2, low coercive field (E_c) of 25 kV/cm, $\varepsilon_r = 1323$, $\tan\delta = 0.045$, Lotgering factors (f) of 0.73, and energy-storage density of 0.12 J/cm^3 at 46.3 kV/cm.

Key words: $Bi_4Ti_3O_{12}$ templates, BNKT ceramics, energy storage density, template grain growth method

INTRODUCTION

In the recent past, lead-free piezoelectric ceramic materials have led to the discovery of numerous advanced ceramics with good physical properties, and have been extensively investigated for functional device applications.[1] Hence, it has become an important topic, and various lead-free piezoelectric ceramics strategies have been explored for replacing the widely-used lead-based ceramics because of their good environmentally friendly properties during the preparation process.[2] In addition, the structure of the pure $Bi_{0.5}(Na_{(1-x)}K_x)_{0.5}TiO_3$ (BNKT) ceramics can be modified, and their properties can also be improved by doping[3,4] or by a fabrication process.[3,5,6] Furthermore, $Bi_4Ti_3O_{12}$ at a content of 7 wt% resulted in a large signal piezoelectric coefficient d_{33}^* and strain hysteresis, η, of 600 pm/V and 36%, respectively, in $Bi_{0.5}(Na_{0.82}K_{0.18})_{0.5}TiO_3$ ceramics.[7] However, the conventional solid-state reaction method leads to random grain orientation; thus, their electrical properties are lower than single-crystal ceramic materials. Especially, the textured ceramics could be made at a low cost compared to their single-crystal equivalent, and anisotropic features similar to a single crystal can be obtained. Recently, enhancements in the dielectric, piezoelectric, and ferroelectric properties of textured ceramics have been reported in textured BNKT,[8,9] BNKT-BT,[3,9] and BCZT[10,11] ceramics,

where different templates were used. In this work, textured $(1 − x)[Bi_{0.5}(Na_{0.4}K_{0.1})TiO_3]$-$xBi_4Ti_3O_{12}$ ceramics were fabricated by a tape-casting method with pure-phase $Bi_4Ti_3O_{12}$ templates, and the optimal contents of $Bi_4Ti_3O_{12}$ templates to form a textured BNKT lead-free ceramic with improved dielectric and ferroelectric properties were determined.

EXPERIMENTAL

Lead-free $(1 − x)[Bi_{0.5}(Na_{0.4}K_{0.1})TiO_3]$-$xBi_4Ti_3O_{12}$ (BNKT-BiT; with $x = 0$, 0.05, 0.10, 0.15, 0.20, and 0.25) ceramics were successfully synthesized by using a reactive templated grain growth method. Bi_2O_3, TiO_2, Na_2CO_3, and K_2CO_3 powders (with purities $\geq 99.5\%$) were used as raw materials.

First, $Bi_4Ti_3O_{12}$ (BiT) templates were synthesized through a molten salt method using Na_2CO_3 and K_2CO_3; TiO_2 nanoparticles were obtained by an ultrasound-assisted method using TiO_2 commercial particles and sulfuric acid.[12,13] The as-prepared $Bi_4Ti_3O_{12}$ templates were composed of plate-like morphologies of lengths 5–20 μm and widths 0.5–1 μm (Fig. 1a). X-ray diffraction (XRD) analysis revealed the orthorhombic perovskite structure of the $Bi_4Ti_3O_{12}$ templates and no other impurities were seen at the temperature of 1050°C (Fig. 1b), similar to those reported in the literature for the $Bi_4Ti_3O_{12}$ crystal.[14]

Secondly, the raw materials of Bi_2O_3, Na_2CO_3, K_2CO_3, and TiO_2 were weighed according to their chemical formulas and then ball-milled for 24 h in anhydrous ethanol with zirconia balls. This sludge was calcined at 850°C for 2 h after drying at 100°C to synthesize BNKT compounds. Powder mixtures containing the matrix particles and $Bi_4Ti_3O_{12}$ templates were mixed with a binder and were tape-cast to form sheets in which the $Bi_4Ti_3O_{12}$ templates were aligned with their plate face parallel to the sheet surface. The amount of the $Bi_4Ti_3O_{12}$ templates was 0 ÷ 0.25 mol, as indicated in the abbreviation of the samples, e.g., BNKT-xBiT).

As the final step, the sheets were then cut, stacked, and pressed in order to form green compacts (Fig. 2). To remove the organic binders in the green compacts, which affect the quality of the ceramic after sintering, the samples were heat-treated at 550°C for 2 h (Fig. 3), similar to our previous report.[2] At the end of the process of fabrication for the BNKT ceramics by the template grain growth method, the textured microstructure was achieved.

The phase structure of the prepared samples was measured by XRD (Rigaku RINT 2000), and the degree of orientation of the ceramics was calculated using the XRD data.[15] Field-emission scanning electron microscopy (Nova NanoSEM) was employed to examine the morphologies of the as-prepared ceramics.[15] Before electrical measurements, the density of the samples was measured by the Archimedes method. Furthermore, the samples were polished to achieve 0.2 mm thickness and then coated with silver electrodes. The ferroelectric hysteresis loops were measured by the Sawyer–Tower method. Finally, the temperature dependence of the dielectric constant and dielectric loss was determined using a RLC meter (HIOKI 3532) with automatic programming.

RESULTS AND DISCUSSION

Table I lists the densification factors of the ceramics at different contents of $Bi_4Ti_3O_{12}$, which were determined using an equation described previously.[16] The densification factor increases with an increase in the content of the $Bi_4Ti_3O_{12}$ templates and achieves the greatest value of DF 0.96 at a BiT content of 0.15 mol, and then increases. The variation in the densification factor of the BNKT-BiT ceramics during sintering can be explained by defect chemistry and the creation of oxygen vacancies. As is well known, Na^+, K^+, and Bi^{3+} volatilize during the sintering process. The volatilization of the ions produces oxygen vacancies in the ceramics according to the Kröger–Vink equation, as follows[17]:
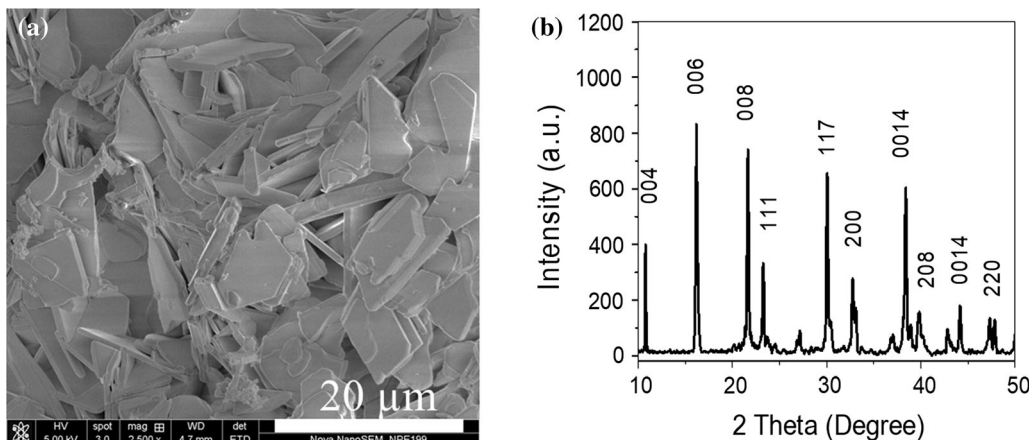

Fig. 1. Characteristics of $Bi_4Ti_3O_{12}$ template: (a) microstructure; (b) crystal structure.

Fabrication of $Bi_{0.5}(Na_{0.4}K_{0.1})TiO_3$ Lead-Free Ceramics Using Reactive Templated Grain Growth Method
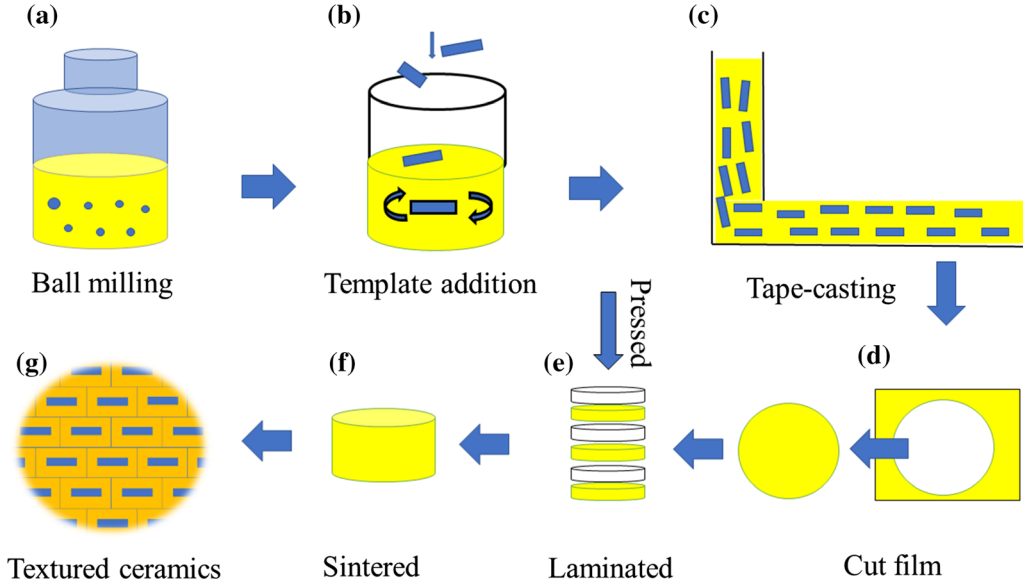

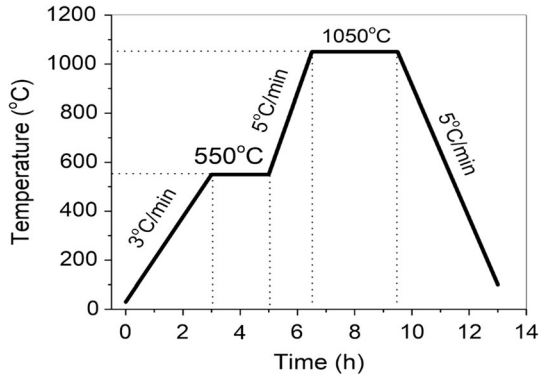Fig. 2. The process of fabrication for $(1 - x)$BNKT-xBiT ceramics by the template grain growth method.

Fig. 3. Diagram of the sintering process.

$$2K_K^x + O_O^x \rightarrow 2K_K' + V_O^{oo} + K_2O \qquad (1)$$

$$2Na_{Na}^x + O_O^x \rightarrow 2Na_{Na}' + V_O^{oo} + Na_2O \qquad (2)$$

$$2Bi_{Bi}^x + O_O^x \rightarrow 2Bi_{Bi}''' + 3V_O^{oo} + Bi_2O_3 \qquad (3)$$
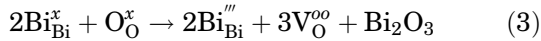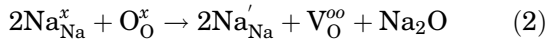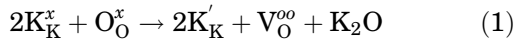
whereby the presence of oxygen vacancies in materials is advantageous for mass transport during sintering in ceramics. The density of the ceramic samples increases with an increase in the content of the $Bi_4Ti_3O_{12}$ platelets, and reaches the highest value of 6.19 g/cm^3 (relative density of 98% of the theoretical value at $x = 0.15$), and then it decreases significantly beyond this point. Table I also expresses the dielectric constant (ε_r) and the dielectric loss (tanδ) of BNKT ceramics measured at room temperature at 1 kHz for different contents of the $Bi_4Ti_3O_{12}$. The ε_r value increases rapidly with an increase in the content of the $Bi_4Ti_3O_{12}$ templates, whereas the tanδ value decreases rapidly when the

amount of $Bi_4Ti_3O_{12}$ templates is less than 0.15 mol. The following optimized values were obtained at $x = 0.15$: $\varepsilon_r = 1323$ and tan$\delta = 0.045$. This can be explained by the texturing characteristics of the ceramics, where the orientation of the plate-like grains is similar to that obtained by the tape-casting method.[18] Ullah et al.[19] suggested that the improvement in the dielectric constant can be ascribed to the high density, larger grain size, and improvement in crystalline quality.

As shown in Fig. 4, in order to study the orientation of the $(1 - x)$[$Bi_{0.5}$ $(Na_{0.4}K_{0.1})TiO_3$]-xBi_4-Ti_3O_{12} ceramics, experiments were conducted to characterize the evolutions of grain microstructures and textures at different contents of $Bi_4Ti_3O_{12}$ platelets. The grain sizes of random BNKT compounds sintered at 1150°C for 2 h were found to be about 1 μm (Fig. 4a). In the case of the $(1 - x)$[$Bi_{0.5}$ $(Na_{0.4}K_{0.1})TiO_3$]-$xBi_4Ti_3O_{12}$ ceramics, plate-like BNKT ceramics were formed by the reaction of the $Bi_4Ti_3O_{12}$ platelets with Na_2CO_3, K_2CO_3, and TiO_2 during the sintering process.[20] In other words, the $Bi_4Ti_3O_{12}$-added ceramics were composed of two types of BNKT grains with different shapes, such as rectangular and plate-like grains.[20] This is the reason that the average grain size of BNKT-BIT ceramics was about ten times larger than those of random BNKT ceramics (Fig. 4b–f). A large amount of equiaxed grains with small sizes were present in the samples containing 0.05 mol and 0.1 mol of the $Bi_4Ti_3O_{12}$ templates, as shown in Fig. 4b and c. However, a small amount of the $Bi_4Ti_3O_{12}$ templates was not sufficient to guide the ceramic particles. It is evident from Fig. 4d–f that the BNKT ceramics with the $Bi_4Ti_3O_{12}$ additive $(0.1 \leq x)$ showed that the size, shape, and uniformity of the ceramic grains are obviously manifested with the increasing concentrations of the templates, and that

Table I. Density, densification, Lotgering factor, dielectric constant, and dielectric loss of $(1 - x)$BNKT-xBiT ceramics

Samples	Density (g/cm^3)	Theoretical density	Relative density (%)	Densification factor	Lotgering factor (%)	ε	$\tan\delta$
BNKT-0.00BiT	5.60	6.01	93.3	0.84	19	986	0.078
BNKT-0.05BiT	5.79	6.11	94.7	0.88	51	1117	0.058
BNKT-0.10BiT	6.08	6.21	97.9	0.95	65	1291	0.046
BNKT-0.15BiT	6.19	6.31	98.0	0.96	73	1323	0.045
BNKT-0.20BiT	6.03	6.42	94.0	0.87	54	1244	0.048
BNKT-0.25BiT	5.94	6.52	91.1	0.81	31	1194	0.053
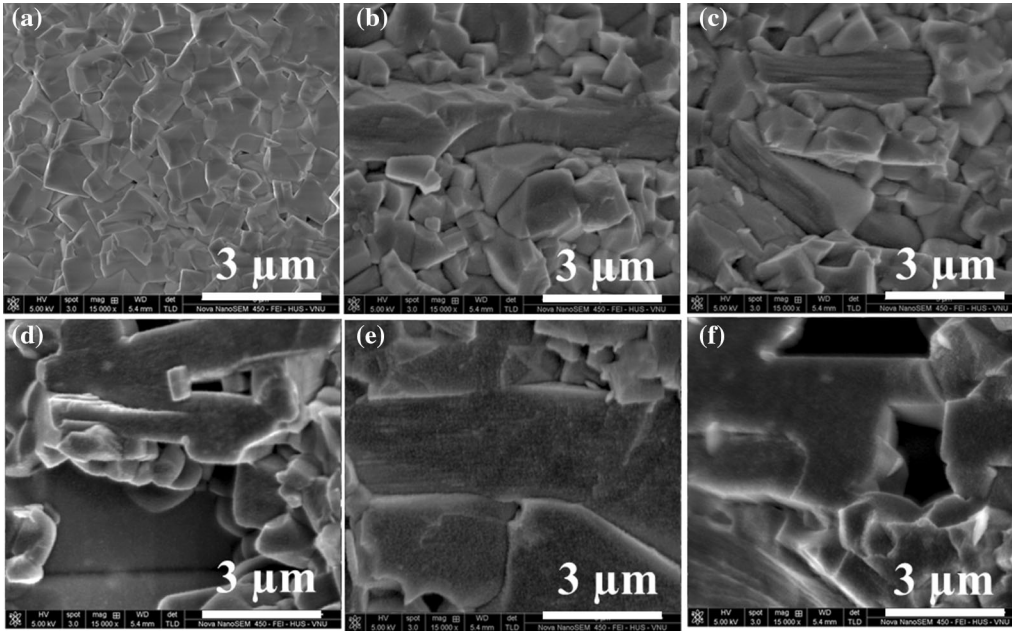
Fig. 4. Fracture surface microstructures of the $(1 - x)$BNKT-xBiT ceramics: (a) $x = 0.0$; (b) $x = 0.05$; (c) $x = 0.10$; (d) $x = 0.15$; (e) $x = 0.20$; (f) $x = 0.25$.

the grains grow apparently with orientation, as demonstrated in Fig. 4d–f. Moreover, it is also observed that the large ceramic grains with the same orientation as that of the templates grow at the expense of other smaller matrix grains. Wu et al.[21] suggested that the existence of the surface of each film and due to the effect of surface tension, the templates should have their major surface aligned parallel to the casting plane, which is beneficial for the texture development. $Bi_4Ti_3O_{12}$ improves the uniformity of the grain size of the ceramics because $Bi_4Ti_3O_{12}$ effectively decreases the sintering temperature and controls the volatilization of the K and Na elements.[22] As discussed, the textured BNKT-BiT ceramics produce brick-layer-like quadrangular grains, which align parallel to the tape-casting direction. While studying textured $0.88Na_{0.5}Bi_{0.5}TiO_3$-$0.08K_{0.5}Bi_{0.5}TiO_3$-$0.04BaTiO_3$ ceramics, Dong et al.[9] suggest that the development of the BNKT

phase formed around the oriented $Bi_4Ti_3O_{12}$ particles. Large particle formation mechanisms in the textured BNKT ceramics may be considered to be solid-state spreading, which results in the growth of the large template grains at the cost of the small-grain matrix.[23] This can be explained by the fact that, in the template grain growth method, the templated grains are grown by using the Ostwald ripening process of two-phase mixtures,[24] which depends on the difference in the grain size between the template and the matrix. The larger templated grains are energetically more stable as compared to the smaller matrix grains. The small matrix grains tend to dissolve and diffuse into the surface of the large templated grains, leading to a continuous growth.[25] The third grains were formed between the $Bi_4Ti_3O_{12}$ templates and $Bi_{0.5}(Na_{0.4}K_{0.1})TiO_3$ particles, and grooves were observed between the $Bi_{0.5}(Na_{0.4}K_{0.1})TiO_3$ particles and the third grains. In

summary, the mechanism of the formation of the large grains is not neck growth[26] but solid-stage spreading, similar to other BNKT ceramics.[27]

In order to determine the structure and the degree of orientation of textured BNKT-BIT ceramics, x-ray diffraction was measured in the 2θ range of 20°–65°, as shown in Fig. 5. The study reveals a pure perovskite phase for all the ceramic samples and thus confirms the dissolution of the $Bi_4Ti_3O_{12}$ templates into the lattice structure of the BNKT in order to form a homogeneous solid solution. However, when the content of the $Bi_4Ti_3O_{12}$ templates exceeds 0.25 mol, an excess $Bi_4Ti_3O_{12}$ phase appears. This can be explained by the solubility limit of $Bi_4Ti_3O_{12}$ in $(1 - x)[Bi_{0.5} (Na_{0.4}K_{0.1})TiO_3]$-$xBi_4Ti_3O_{12}$ ceramics. The visible (100) and (100) non-split peaks at the 2θ of around 22° and 46°, respectively, proved that a pseudocubic symmetry appears over the entirety of the studied samples. According to many published works on the structure of the randomly axed BNKT ceramics,[3,28] the peak intensity of the (110) reflection at $2\theta \approx 32.45°$ is the greatest. Compared with the randomly axed BNKT ceramics, samples fabricated by the template grain growth method presented significantly enhanced (100) and (200) diffraction peaks with an increase in the content of the $Bi_4Ti_3O_{12}$ templates.

The texture fraction, calculated from the Lotgering factor[15] (f, Eq. 4) is listed as a function of $Bi_4Ti_3O_{12}$ templates in Table I.

$$f = \frac{P - P_o}{1 - P_o} \quad (4)$$

where $P = \frac{\sum I(00l)}{\sum I(hkl)}$, $P_o = \frac{\sum I(00l)}{\sum I(hkl)}$ whereas $\sum I(00l)$ and $\sum I(hkl)$ are the sums of the intensities of the $(00l)$ and (hkl) reflections, respectively, and P_o is the value of P for a random powder sample used in the study. In the x range from 0.0 to 0.25, the Lotgering factors (f) exhibited values of 0.19, 0.51, 0.65, 0.73, 0.54, and 0.31 for the BNKT-BiT ceramics, respectively (Table I). Moreover, the Lotgering factor of the textured BNKT prepared with 0.15 mol of

Fig. 5. X-ray diffraction of the $(1 - x)$BNKT-xBiT ceramics was measured in the 2θ range of 20°–65°.

$Bi_4Ti_3O_{12}$ templates was 73%, which is much higher compared to that of the non-textured BNKT (0%), as shown in Table I. Jing et al.[29] reported that $Bi_{0.5}(Na_{1-x}K_x)_{0.5}TiO_3$ with an orientation factor increased from 2.73% to 26.41% when the template concentration increased from 10% to 40%. An orientation degree of 60% for $Bi_{0.5}Na_{0.35}K_{0.1}Li_{0.05}$-$TiO_3$ ceramics was obtained at 1085°C after 12 h.[30] According to Cha et al.,[31] the Lotgering factor of the textured $Bi_{0.5}(Na_{0.5}K_{0.5})_{0.5}TiO_3$ prepared with 12 mol of the $Bi_{4.5}Na_{0.5}Ti_4O_{15}$ template was about 65%. The f value of $0.94Bi_{0.5}Na_{0.5}TiO_3$-$0.06BaTiO_3$ ceramics can reach up to 70%.[32] However, when the content of $Bi_4Ti_3O_{12}$ templates is higher than 0.25 mol, the $Bi_4Ti_3O_{12}$ phase appeared, which resulted in the partial return of the orientation and a decrease in the degree of orientation.

The crystal structure of BKNT ceramics with different $Bi_4Ti_3O_{12}$ contents can be analyzed by changes in the phonon behavior of the Raman spectra identified as changes in the frequency or intensity of the peaks. Figure 6 shows the Raman spectroscopy from 80 cm^{-1} to 1000 cm^{-1} deconvoluted using a Gaussian–Lorentzian function. As can be seen in Fig. 6, the four main regions can be detected the high-frequency region (> 700 cm^{-1}), between 400–700 cm^{-1}, between 200–400 cm^{-1}, and below 200 cm^{-1}.

The first band region, i.e., the peak centered between 96 cm^{-1} and 102 cm^{-1}, can be assigned to in the A_1 (TO) mode, which is associated with the A-site vibrations, and Bi-O, Na-O, and K-O bonds,[33] and is found to be sensitive to phase changes in the crystal structure of the perovskite.[33] With an increase in the contents of the $Bi_4Ti_3O_{12}$ templates, the A-site mode tends to reduce in the wavenumber, as shown in Fig. 7a. Thus, it can explain that the $Bi_4Ti_3O_{12}$ templates get dissolved into the BNKT lattice and hence affect the vibrations of the A-site perovskite, and may also induce a phase transition.[7] In contrast, Bi-O vibrations are expected at lower wavenumbers because the mass of Bi is higher as compared to the other cations.[33] However, with an increase in the contents of the $Bi_4Ti_3O_{12}$ templates, the A-site mode tends to increase the full width at half-maximum (FWHM), as shown in Fig. 7b. It has been suggested that the Bi^{3+} ion ($R_{Bi} \sim 1.17$ Å) has a smaller ionic radius as it enters the A site of the perovskite unit cell in order to replace the Na$^+$ and K$^+$ ions ($R_{Na} \sim 1.39$ Å) and the K$^+$ ($R_K \sim 1.64$ Å) ions, which induces changes in the lattice structure.[22] The second region is located in the range of 200–400 cm^{-1} and can stem from the vibration of the Ti-O bond, and the region located around 266 cm^{-1} is associated with the tetragonal phase in the perovskite structure.[34–36]

Meanwhile, the bands located in a frequency range of 450–650 cm^{-1} are associated with the TiO6 octahedron vibration mode, and are dominated by vibrations that mainly involve oxygen displacements. They become increasingly distinct with an
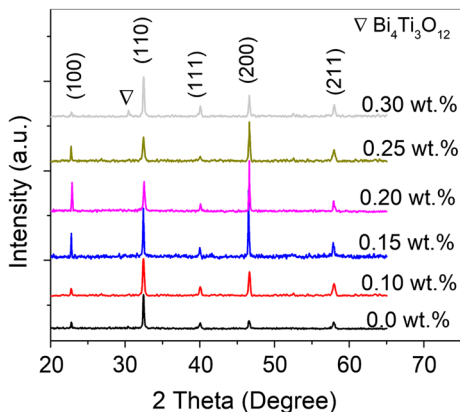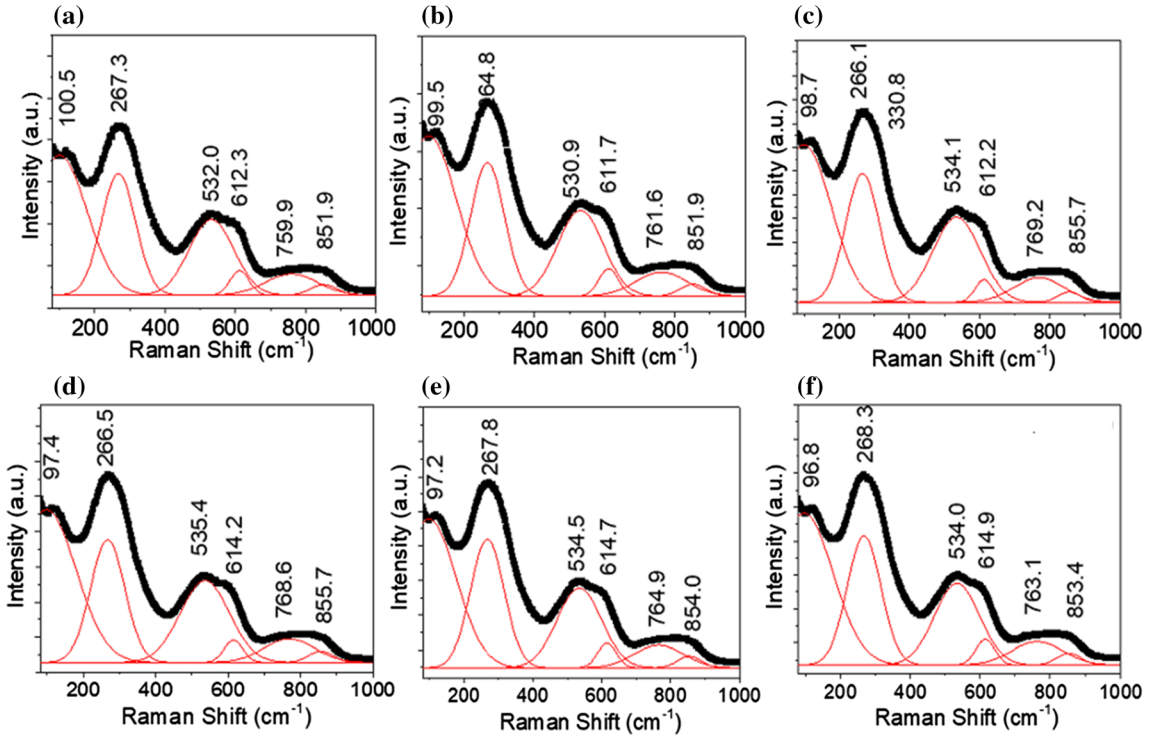
Fig. 6. Raman spectra of $(1 - x)[Bi_{0.5}(Na_{0.4}K_{0.1})TiO_3]$-$xBi_4Ti_3O_{12}$ ceramics: (a) $x = 0.0$; (b) $x = 0.05$; (c) $x = 0.10$; (d) $x = 0.15$; (e) $x = 0.20$; (f) $x = 0.25$.
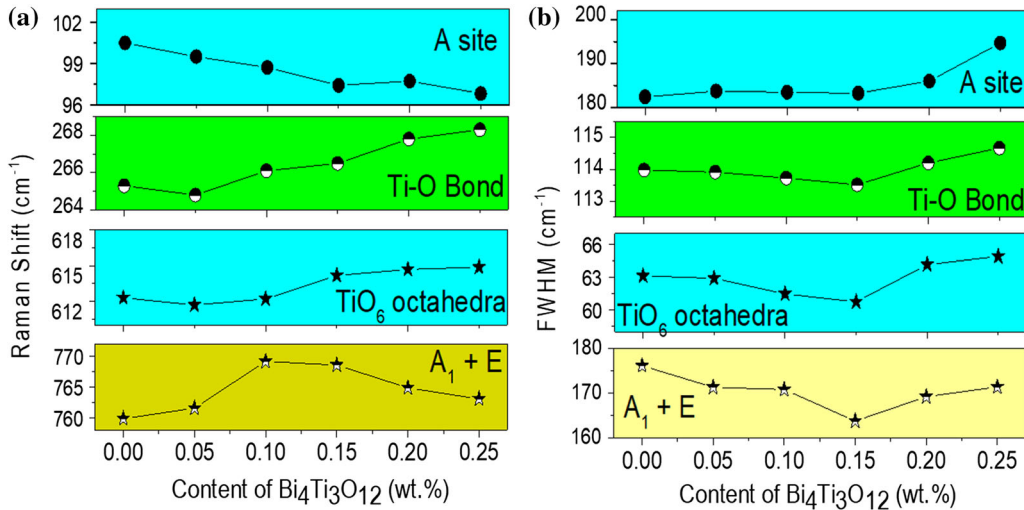

Fig. 7. Results of the position of Raman vibrational modes (a) and FWHM (b).

increase in the x content. Hence, this result demonstrates a particular phonon behavior in structural evolution.[37] Moreover, both the modes of the TiO_6 octahedra and the Bi-O bond demonstrate an increase in the wavenumber with an increase in the contents of the $Bi_4Ti_3O_{12}$ templates (Fig. 7a). The FWHM of the Bi-O bond and TiO_6 octahedra modes decreases when the value of x changes from 0 to 0.15, while, with a further increase in $Bi_4Ti_3O_{12}$ content, the width of the modes increases (Fig. 7b). The broadband observed in the fourth region could

originate from the A_1 (LO) and E (LO) overlapping bands. Moreover, the presence of broader peaks is associated with the presence of oxygen vacancies.[36] In this mode, the wavenumber first increases and reaches the highest value at $Bi_4Ti_3O_{12}$ content of 0.15, and then decreases, while the FWHM of this mode follows the opposite direction. The FWHM of the A_1 + E mode decreases when the value of x changes from 0 to 0.15. However, the FWHM of the A_1 + E mode increases when x increases beyond 0.15 (Fig. 7b). Furthermore, the changes in the

wavenumber of the vibrational modes, width, and Raman peak distances are always associated with structural changes. This is consistent with many published works,[2,38] and the above-mentioned XRD analysis results.

In order to explore the diffusion phase transition characteristics of the textured BNKT and random BNKT ceramics, the temperature-dependence of their dielectric constant (ε_r) and the dielectric loss ($\tan\delta$) were measured at 1 kHz from room temperature to 370°C (Fig. 8). There appear three dielectric anomalies in the curves, denoted T_d, T_p, and T_m, corresponding to increasing temperature. Recent studies on the basis of BNKT ceramics reported that the depolarization temperature (T_d) corresponds to the temperature of the first $\tan\delta$ peak. According to Lu et al.,[39] the temperature T_d corresponds to the ferroelectric–relaxor transition. It has been suggested that T_d should be lower than the temperature range of energy-storage applications to obtain a large energy density. The textured ceramic exhibited T_d and T_p temperatures, which are lower than those of the random ceramics. As for the T_p anomaly, since it is a relaxation behavior, this may broaden the temperature stability range of energy storage.[39] The third peak at higher temperatures corresponds to the ferroelectric–paraelectric phase transition temperature (the T_m Curie temperature). Both the ceramics were found to be relatively broad, which indicates a diffuse phase transition at T_m.[28] As described in Fig. 8, the presence of $Bi_4Ti_3O_{12}$ in the oriented ceramics exhibited a higher value of T_m as compared to that for non-textured ceramics. This difference is due to the phase transformation temperatures between non-textured BNKT ceramics ($T_m \sim 261°C$) and $Bi_4Ti_3O_{12}$ ceramics ($T_m \sim 675°C$),[40] so the dielectric constant peak of the textured BNKT ceramics increases and becomes sharp (lower γ value). Here, γ is the degree of diffuseness and C is the Curie-like constant. The value of γ ranges from 1 (normal ferroelectric) to 2 (ideal relaxor ferroelectric).[41] The values of the maximum dielectric constant (ε_{max}) of the textured BNKT and random BNKT ceramics at T_m were 6680 and 5298, respectively.

Figure 9 displays the P–E hysteresis loops of random and textured BNKT-BiT ceramics with 0.15 mol BiT templates. The textured samples exhibited a high remnant polarization ($P_r = 16$ μC/cm^2) and a low coercive field ($E_c = 25$ kV/cm) (Fig. 9a) compared to those of the random samples ($P_r = 13.1$ μC/cm^2; $E_c = 29.8$ kV/cm) (Fig. 9b). Improvements in the degree of orientation of BNKT ceramics were thought to be the causes for the improvement of the ferroelectric properties of the ceramics because the E_c of the textured ceramics is usually lower than that of the non-textured ceramics.[2,42] The energy storage density (W_1) was obtained by using the unipolar P–E hysteresis loops, as shown in Eq. 5.[39,43]:

$$W_1 = \int_{P_r}^{P_{max}} E\,\mathrm{d}P \qquad (5)$$

and the energy loss density W_2 is obtained by integrating the area between the charge and discharge curves, as shown in Fig. 9a and b. The energy storage efficiency (η) of the nonlinear dielectric materials is usually calculated according to Eq. 6.[39,43]:

$$\eta = \frac{W_1}{W_1 + W_2} \qquad (6)$$

The comparison energy-storage behaviors of the textured BNKT-BiT and random ceramics are shown in Fig. 9. As illustrated in Fig. 9a and b, the ferroelectric state maintains a high remnant polarization, P_r, which results in a low reversible energy storage density. The textured BNKT-BiT ceramic exhibited higher energy density W_1 (0.12 J/cm^3) and energy loss density W_2 (0.61 J/cm^3) than those of the random ones ($W_1 = 0.08$ J/cm^3,
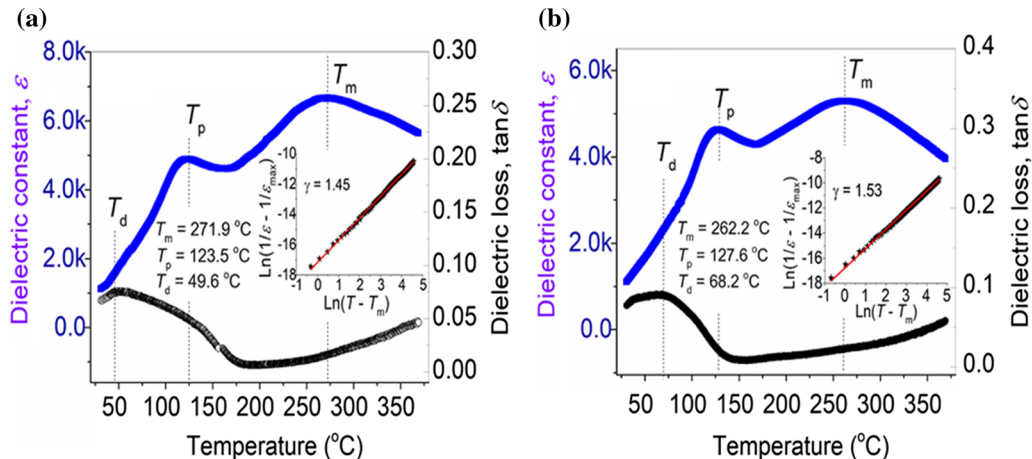

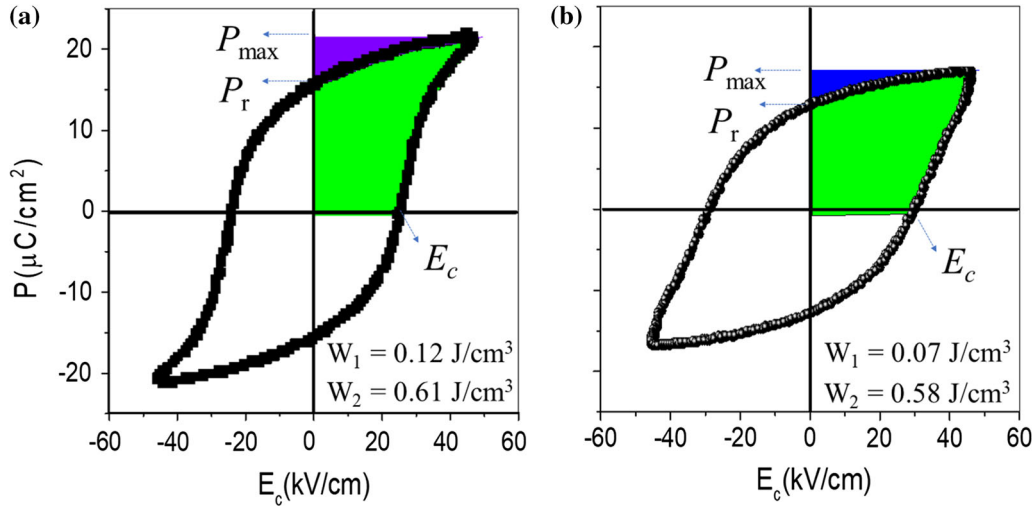Fig. 8. Temperature-dependence of ε_r and $\tan\delta$ of the (a) textured BNKT and (b) random BNKT ceramics.

Fig. 9. *P–E* hysteresis loops and the energy storage properties of the (a) textured BNKT and (b) random BNKT ceramics.

$W_2 = 0.58$ J/cm^3) at 46.3 kV/cm (Fig. 9b and c). This clearly indicates that the energy storage efficiency (η) in the textured BNKT is higher than that of random ceramics (0.17 and 0.11, respectively). Briefly, the texture displays a significant effect on the dielectric and ferroelectric properties: the highly textured ceramics exhibited ε_{max} values higher by 25.9% and P_r values higher by 22.1% as compared to those of the non-textured ceramics, which can be explained by the large grain size, high density of the samples, and high crystal orientation.

CONCLUSIONS

Lead-free $(1 - x)[Bi_{0.5}(Na_{0.4}K_{0.1})TiO_3]$-$xBi_4Ti_3O_{12}$ ceramics were successfully synthesized by using a reactive templated grain growth method for improving their preferred degree of orientation, dielectric, and ferroelectric properties. In this way, a high-degree orientation of 73% was obtained in the textured BNKT ceramics using 0.15 mol Bi$_4$Ti$_3$O$_{12}$ templates with the following optimal properties: a dielectric constant ε_{max} of 6680, a high remnant polarization P_r of 16 μC/cm^2, a low coercive field E_c of 25 kV/cm, $\varepsilon_r = 1323$ and $\tan\delta = 0.045$, and an energy-storage density of 0.12 J/cm^3 at 46.3 kV/cm. According to the obtained results, the 0.85[Bi$_{0.5}$ (Na$_{0.4}$K$_{0.1}$)TiO$_3$]-0.15Bi$_4$Ti$_3$O$_{12}$ ceramics will be promising candidates for various applications.

CONFLICT OF INTEREST

All persons who meet authorship criteria are listed as authors, and all authors certify that we have participated sufficiently in the work to take public responsibility for the content, including participation in the concept, design, analysis, writing, or revision of the manuscript and the authors declare that they have no conflict of interest.

REFERENCES

1. B. Yan, H. Fan, C. Wang, M. Zhang, A.K. Yadav, X. Zheng, H. Wang, and Z. Du, *Ceram. Int.* 46, 281–288 (2020).
2. L. Dai Vuong and A.Q. Dao, *J. Electroceram.* 44, 68–77 (2020).
3. L.D. Vuong and P.D. Gio, *J. Alloys Compd.* 817, 152790 (2020).
4. Y. Pu, M. Yao, L. Zhang, and P. Jing, *J. Alloys Compd.* 687, 689–695 (2016).
5. P. Butnoi, S. Manotham, P. Jaita, C. Randorn, and G. Rujijanagul, *J. Eur. Ceram. Soc.* 38, 3822–3832 (2018).
6. P. Butnoi, S. Manotham, and T. Tunkasiri, *Key Eng. Mater.* 798, 212–217 (2019).
7. P. Fan, Y. Zhang, Q. Zhang, B. Xie, Y. Zhu, M.A. Mawat, W. Ma, K. Liu, J. Xiao, and H. Zhang, *J. Eur. Ceram. Soc.* 38, 4404–4413 (2018).
8. T. Shoji, K. Fuse, and T. Kimura, *J. Am. Ceram. Soc.* 92, S140–S145 (2009).
9. N. Dong, X. Gao, F. Xia, H. Liu, H. Hao, and S. Zhang, *Crystals* 9, 206 (2019).
10. S.K. Ye, J.Y.H. Fuh, and L. Lu, *Appl. Phys. Lett.* 100, 252906 (2012).
11. K. Jai Shree and D. Das, *J. Mater. Sci. Mater. Electron.* 30, 11094–11107 (2019).
12. D.N. Trung, V.L. Dai, S.N. Manh, V.T. Ho, and V.C. Truong, *Nanomater. Energy* 6, 82–88 (2017).
13. L.D. Vuong, *Nanotechnology for Agriculture: Crop Production & Protection*, ed. D.G. Panpatte and Y.K. Jhala (Singapore: Springer, 2019), pp. 85–106.
14. G.A. Geguzina, A.T. Shuvayev, V.G. Vlasenko, E.T. Shuvayeva, and L.A. Shilkina, *Crystallogr. Rep.* 48, 406–412 (2003).
15. F. Lotgering, *J. Inorg. Nucl. Chem.* 9, 113–123 (1959).
16. M.S. Alkathy, A. Hezam, K. Manoja, J. Wang, C. Cheng, K. Byrappa, and K.J. Raju, *J. Alloys Compd.* 762, 49–61 (2018).
17. T. Wang, X.-M. Chen, and Y.-Z. Qiu, *Ferroelectrics* 510, 161–169 (2017).
18. A. Hussain, C.W. Ahn, H.J. Lee, I.W. Kim, J.S. Lee, S.J. Jeong, and S.K. Rout, *Curr. Appl. Phys.* 10, 305–310 (2010).
19. A. Ullah, C.W. Ahn, A. Hussain, and I.W. Kim, *Curr. Appl. Phys.* 10, 1367–1371 (2010).
20. C.W. Ahn, E.D. Jeong, Y.H. Kim, J.-S. Lee, H.J. Lee, and I.W. Kim, *J. Electroceram.* 23, 402 (2009).

Fabrication of Bi$_{0.5}$(Na$_{0.4}$K$_{0.1}$)TiO$_3$ Lead-Free Ceramics Using Reactive Templated Grain Growth Method

21. M. Wu, Y. Li, D. Wang, J. Zeng, and Q. Yin, *J. Electroceram.* 22, 131–135 (2009).
22. Z.-J. Dong, Y.-P. Pu, and Y.-W. Liu, *Ceram. Int.* 43, S55–S58 (2017).
23. D.-D. Wei, Q.-B. Yuan, G.-Q. Zhang, and H. Wang, *J. Mater. Res.* 30, 2144–2150 (2015).
24. P.W. Voorhees, *Annu. Rev. Mater. Sci.* 22, 197–215 (1992).
25. Y. Yan, K.H. Cho, and S. Priya, *J. Am. Ceram. Soc.* 94, 1784–1793 (2011).
26. D. Demirskyi, H. Borodianska, D. Agrawal, A. Ragulya, Y. Sakka, and O. Vasylkiv, *J. Alloys Compd.* 523, 1–10 (2012).
27. Z.-H. Zhao, M.-Y. Ye, H.-M. Ji, X.-L. Li, X. Zhang, and Y. Dai, *Mater. Des.* 137, 184–191 (2018).
28. L.D. Vuong and N. Truong-Tho, *J. Electron. Mater.* 46, 6395–6402 (2017).
29. X. Jing, Y. Li, Q. Yang, J. Zeng, and Q. Yin, *Ceram. Int.* 30, 1889–1893 (2004).
30. W.K. Tam, K.W. Kwok, J.T. Zeng, and H.L.W. *Chan, J. Phys. D Appl. Phys.* 41, 045402 (2008).
31. H.A. Cha, Y.-K. Kim, and J.-H. Jeon, *J. Eur. Ceram. Soc.* 37, 967–974 (2017).
32. J. Zhao, F. Wang, W. Li, H. Li, D. Zhou, S. Gong, Y. Hu, and Q. Fu, *J. Appl. Phys.* 108, 073535 (2010).
33. D. Fernandez-Benavides, A. Gutierrez-Perez, A. Benitez-Castro, M. Ayala-Ayala, B. Moreno-Murguia, and J. Muñoz-Saldaña, *Materials* 11, 361 (2018).
34. S. Bhandari, N. Sinha, G. Ray, and B. Kumar, *CrystEngComm* 16, 4459–4466 (2014).
35. T.H. Kim, S. Kojima, C.W. Ahn, I.W. Kim, and J.-H. Ko, *J. Korean Phys. Soc.* 62, 1009–1013 (2013).
36. G. Hernandez-Cuevas, J.R. Leyva Mendoza, P.E. García-Casillas, C.A. Rodríguez González, J.F. Hernandez-Paz, G. Herrera-Pérez, L. Fuentes-Cobas, S.D. de la Torre, O. Raymond-Herrera, and H. Camacho-Montes, *J. Adv. Ceram.* 8, 278–288 (2019).
37. J. Hao, Z. Xu, R. Chu, W. Li, P. Fu, and J. Du, *J. Alloys Compd.* 677, 96–104 (2016).
38. N.D. Quan, N. Van Hong, T.Q. Toan, and V.N. Hung, *Eur. Phys. J. B* 91, 316 (2018).
39. X. Lu, J. Xu, L. Yang, C. Zhou, Y. Zhao, C. Yuan, Q. Li, G. Chen, and H. Wang, *J. Materiomics* 2, 87–93 (2016).
40. P. Pookmanee and S.J. Phanichphant, *J. Ceramic Process. Res.* 10(4), 448–452 (2009).
41. L.D. Vuong, P.D. Gio, N.T. Tho, and T.V. Chuong, *Indian J. Eng. Mater. Sci.* 20, 555–560 (2013).
42. M. Wu, Y. Wang, D. Wang, and Y. Li, *IEEE Trans. Ultrason. Ferroelectr. Freq. Control* 58, 2036–2041 (2011).
43. X. Liu, J. Shi, F. Zhu, H. Du, T. Li, X. Liu, and H. Lu, *J. Materiomics* 4, 202–207 (2018).